Snow thickness retrieval from L-band brightness temperatures: a model comparison

Nina MAASS,[1] Lars KALESCHKE,[1] Xiangshan TIAN-KUNZE,[1] Rasmus T. TONBOE[2]

[1]*Institute of Oceanography, University of Hamburg, Hamburg, Germany*
E-mail: nina.maass@zmaw.de
[2]*Danish Meteorological Institute, Copenhagen, Denmark*

ABSTRACT. The Soil Moisture and Ocean Salinity (SMOS) satellite's L-band (1.4 GHz) measurements have been used to retrieve snow thickness over thick sea ice in a previous study. Here we consider brightness temperature simulations for 2.5–4.5 m thick Arctic multi-year ice and compare the results of the relatively simple emission model (M2013) used previously for the retrieval with simulations from a more complex model (T2011) that combines a sea-ice version of the Microwave Emission Model for Layered Snowpacks (MEMLS) with a thermodynamic model. We find that L-band brightness temperature is mainly determined by ice temperature. In the M2013 model, ice temperature in turn is mainly determined by surface temperature and snow thickness, and this dependence has been used previously to explain the potential for a snow thickness retrieval. Our comparisons suggest that the M2013 retrieval model may benefit from a more sophisticated thermodynamic calculation of the ice temperature or from using independent temperature data (e.g. from 6 GHz channels). In both models, horizontally polarized brightness temperatures increase with snow thickness while holding surface temperature, ice thickness and snow density near constant. The increase in the T2011 model is steeper than in M2013, suggesting a higher sensitivity to snow thickness than found earlier.

KEYWORDS: remote sensing, sea ice, snow

INTRODUCTION

The surface energy balance in polar regions is largely determined by the snow on sea ice, mainly due to the high albedo and the low thermal conductivity of snow. Additionally, snow modifies the surface radiative properties of sea ice and thus the signal observed from satellites. More explicitly, information on snow thickness is required for the freeboard-based estimation of sea-ice thickness from lidar and radar altimetry (Giles and others, 2007; Kwok and Cunningham, 2008). In a first study on the potential for retrieving snow thickness from Soil Moisture and Ocean Salinity (SMOS) satellite data, a relatively simple emission model was used to retrieve snow thickness, and these SMOS-retrieved snow thicknesses were compared with airborne snow radar measurements (Maaß and others, 2013). Here we compare this emission model with a more sophisticated combined emission and thermodynamic model (Tonboe and others, 2011) and investigate the implications for a potential snow thickness retrieval from SMOS brightness temperatures.

To date, the most comprehensive snow dataset for the Arctic Ocean is based on snow thickness and density measurements from Soviet drifting stations between 1954 and 1991 (Warren and others, 1999). However, it is not clear how well this climatology represents present-day snow conditions (Kurtz and Farrell, 2011). Recent changes in the Arctic hydrological cycle have been observed to result in a pronounced decline in summer snowfall over the Arctic Ocean and the Canadian Arctic Archipelago during 1989–2009 (Screen and Simmonds, 2012), and model projections have suggested a considerable decline in spring snow thickness over the 21st century (Hezel and others, 2012). While the airborne radar measurements of NASA's Operation IceBridge mission provided the first cross-basin surveys of snow thickness over Arctic sea ice (Kwok and others, 2011), airborne remote

sensing is, in general, spatially and temporally restricted to individual campaigns. Continuous retrievals of snow thickness are provided by passive microwave satellite measurements, using the spectral gradient ratio of the 19 and 37 GHz vertical polarization channels (e.g. Markus and Cavalieri, 1998). However, surface roughness variations introduce uncertainties to this method (Stroeve and others, 2006), and the method is only applicable to dry snow conditions and only to Antarctic sea ice and first-year ice in the Arctic, but not to multi-year ice (Comiso and others, 2003).

A first satellite-based method to estimate snow thickness over thick multi-year ice from microwave radiometer measurements used data from the European Space Agency's SMOS mission (Maaß and others, 2013). The SMOS mission carries the first satellite-based passive microwave radiometer that continuously measures radiation emitted from the Earth at a frequency of 1.4 GHz in the L-band. The mission was successfully launched in 2009, and, since spring 2010, observations have been made available to scientific and operational users (Mecklenburg and others, 2012). Although designed to provide global estimates of soil moisture and ocean salinity, L-band brightness temperatures measured by SMOS have been used to retrieve thin sea-ice thickness (Kaleschke and others, 2012; Tian-Kunze and others, 2013; Huntemann and others, 2014). In contrast to the retrieval models used to retrieve ice thickness from SMOS in these studies, the emission model presented by Maaß and others (2013) contained a snow layer on top of the sea ice. They used an emission model that is based on the solution of the radiative transfer equation as presented by Burke and others (1979). In their study, implementing a snow cover caused the modeled brightness temperatures on thick sea ice to increase by about 10–13 K at low incidence angles $\theta \leq 15°$, and at higher incidence angles $(50° \leq \theta \leq 60°)$ brightness

temperatures increased by ~ 26 K at horizontal and by 3 K at vertical polarization. According to their model, this increase was caused by low reflectivities at the air/snow and snow/ice boundaries as compared to the reflectivity of the previously considered air/ice boundary. In addition, they found that brightness temperatures in the model increased with snow thickness due to the thermal insulation effect of snow and its dependence on the snow layer thickness. For the considered relatively cold multi-year ice conditions (surface temperature $-33°$C; ice salinity 1.5; snow density 300 kg m^{-3}; ice thickness 4 m) the modeled brightness temperatures at horizontal polarization ($\theta = 45°$) increased by ~ 6 K for a snow thickness increase of 0.40 m. A first sensitivity analysis with the emission model suggested that, within the expected range of variability, the sensitivity of brightness temperature to snow thickness is higher than to the other considered ice parameters. A first comparison of SMOS-retrieved snow thicknesses with airborne snow radar measurements during the Operation IceBridge campaign showed that agreement was best for snow thicknesses less than 0.35 m. For these snow thicknesses and the most suitable assumptions on the ice conditions in the model, average snow thicknesses agreed within 0.1 cm; the root-mean-square deviation was 5.5 cm and the coefficient of determination $r^2 = 0.58$.

Here we try to assess how realistically the relatively simple emission model used in the first SMOS snow thickness retrieval study (Maaß and others, 2013) describes the sensitivity of brightness temperature to snow thickness and the impact of the ice conditions (e.g. ice temperature, snow density, ice salinity). As far as we know, there are no comprehensive measurements of the required ice parameters on a scale comparable to SMOS measurements, which have footprints on the order of 35–50 km. Thus, for comparison we use the output of a more sophisticated model that combines a sea-ice version of the Microwave Emission Model for Layered Snowpacks (MEMLS) with a thermodynamic model (Tonboe and others, 2011). This model takes into account more ice parameters than the simpler model used by Maaß and others (2013) and is driven by meteorological reanalysis data. The MEMLS-based model has been used to simulate a 9 month time series of L-band brightness temperatures ($\theta = 50°$) for multi-year sea ice in the Arctic. Here we use the thermodynamically simulated ice parameters of the combined model to simulate brightness temperatures with our simpler model and compare these brightness temperatures with the MEMLS-based simulations. We investigate whether the previously used relatively simple model is sufficient as a retrieval model or what improvements could be made. Additionally, we use the MEMLS-based model to verify the dependence between L-band brightness temperatures and snow thickness, which is the basis for a potential SMOS snow thickness retrieval over thick sea ice.

MODELS

Emission model for SMOS retrieval

In contrast to the first approaches to retrieve ice thickness from SMOS L-band brightness temperatures (e.g. Kaleschke and others, 2012), the emission model presented by Maaß and others (2013) accounts for a snow layer on top of the ice. This model is referred to as M2013 in the following. The M2013 model is based on the emission model described by Burke and others (1979), which is used to consider a semi-infinite (half-space) layer of air on top, a layer of snow on top

of a layer of ice, and a semi-infinite layer of sea water at the bottom. The emission model describes the brightness temperature above snow-covered sea ice as a function of the water temperature and permittivity, and of the temperatures, permittivities and thicknesses of the snow and the ice layer, respectively. In the model, the permittivities are calculated from empirical relationships. Water permittivity mainly depends on water temperature and salinity (Klein and Swift, 1977). Ice permittivity can be approximately described as a function of brine volume fraction (Vant and others, 1978), which depends on ice salinity and the densities of the ice and the brine (Cox and Weeks, 1983), which in turn mainly depend on ice temperature (Pounder, 1965; Cox and Weeks, 1983). The permittivity of dry snow can be estimated from snow density and snow temperature (Tiuri and others, 1984). If not given as input to the M2013 model, the bulk temperatures of the snow and the ice layer are estimated from the surface temperature, using a simple heat transfer equation (Untersteiner, 1964; Maykut and Untersteiner, 1971) and climatological values for the thermal conductivities of ice and snow (Yu and Rothrock, 1996). As a result, the snow-cover thickness affects the ice temperature in the model. In Maaß and others (2013), this impact is assumed to be the main reason for the (indirect) dependence between the brightness temperature and the snow thickness and is the basis for their snow thickness retrieval over thick ice. Thus, the relationship between ice surface temperature T_{SURFACE} and snow/ice interface temperature $T_{\text{SNOW–ICE}}$ (from which the bulk ice temperature is inferred by assuming a constant temperature gradient in the ice) is essential, and here we apply two different approaches to compare brightness temperatures derived from the M2013 model with those derived from the more sophisticated MEMLS-based model (Tonboe and others, 2011), which is referred to as T2011 throughout this study and is introduced in the next subsection. We compare T2011 brightness temperatures with (1) brightness temperatures as obtained from the M2013 model when using the T2011 model's T_{SURFACE} as input parameter and calculating the ice temperature from the simple heat transfer equation in the M2013 model (denoted by Tb) or with (2) brightness temperatures as obtained from the M2013 model when using both T_{SURFACE} and $T_{\text{SNOW–ICE}}$ from the T2011 simulations as input parameters (denoted by Tb^*). By using the comparisons with Tb^*, we evaluate the potential of the emissivity calculations in the M2013 model independently of the embedded simple heat equation model, whereas Tb is used to identify the difference between the previously used retrieval approach and the T2011 model with regard to the potential for a snow thickness retrieval from L-band measurements.

The input parameters for the M2013 model are sea-water temperature, sea-water salinity, surface temperature (and optionally snow/ice interface temperature), bulk ice salinity, bulk snow density, and the ice and snow thicknesses. For the simulations presented here, we assume that the water has a salinity of 33, is at the freezing point of sea water and has a constant water temperature of $-1.8°$C. In this study, the remaining input parameters of the M2013 model are provided by the T2011 model.

Combined thermodynamic and emission model

Our relatively simple M2013 model presented above is compared to a more sophisticated combined thermodynamic and emission model, which is described by Tonboe
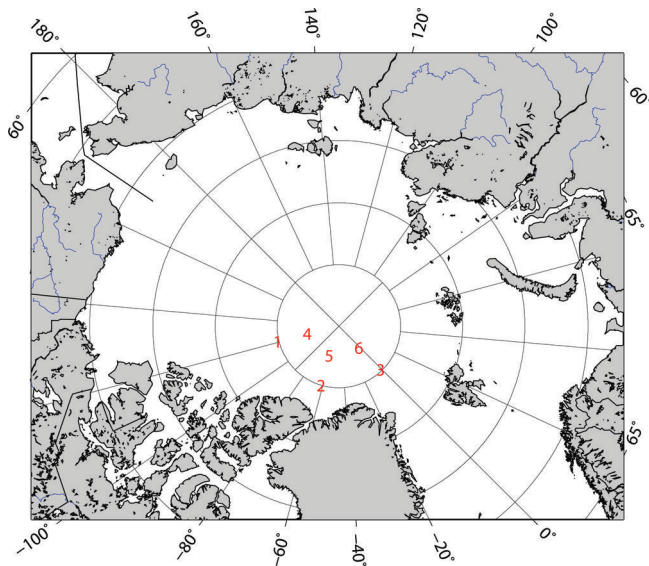
Fig. 1. The six multi-year ice profile positions of the model simulations described in Tonboe and others (2011).

and others (2011). In this T2011 model, a one-dimensional snow and ice thermodynamic model is driven by the European Centre for Medium-Range Weather Forecasts (ECMWF) reanalysis ERA40 data, namely the surface air pressure, the 2 m air temperature, the 10 m wind speed, the incoming shortwave solar radiation and longwave radiation, the dew-point temperature and the precipitation data. The thermodynamic model has been developed to provide realistic microphysical input from these parameters to the emission model. The emission model is a sea-ice version (Tonboe and others, 2006) of MEMLS (Wiesmann and Mätzler, 1999). The T2011 model has a time step of 6 hours. The vertical resolution in the ice is 0.05 m, while the vertical resolution in the snowpack depends on individual precipitation events and the subsequent metamorphosis. The output parameters of the thermodynamic model are, for example, the snow freeboard, snow and ice thickness, the surface density and temperature, the correlation length of the surface snow, the snow/ice interface temperature, the average snow density, the average correlation length of the snow, and the average snow temperature and salinity.

The combined thermodynamic and emission model T2011 was used to simulate the 1.4 GHz brightness temperature at 50° incidence angle at horizontal and vertical polarization for six locations of multi-year ice in the Arctic (Fig. 1). The simulations were performed for the period 1 September 1999 to 31 May 2000 and were initiated with an isothermal 2.5 m thick ice floe at 270 K with a 5 cm thick layer of old snow on top. In each simulation, the ice thickness gradually increases from 2.5 m to almost 4.5 m at the end of the simulation period. The initial salinity profile consists of low salinities (0.5–1.0) in the upper 0.2 m of ice and a constant salinity of 2.5 in the rest of the ice column. The salinity of newly formed ice at the ice/water interface depends on growth rate. As input to the M2013 model we use bulk ice salinity, i.e. the average salinity over the ice column. As new ice forms at the bottom of the multi-year ice, bulk ice salinity gradually increases from 2.4 at the beginning of the simulations to ~3.6 at the end because the relative fraction of the more saline ice formed during current ice growth season gradually increases.

RESULTS

Comparison of brightness temperatures from the two models

Figure 2 shows the time series of the horizontally and vertically polarized brightness temperatures at 1.4 GHz for an incidence angle $\theta = 50°$ as simulated with the T2011 model from 1 September 1999 to 31 May 2000. Additionally, we show the T2011 simulations of the ice parameters that are input parameters to the M2013 model and the brightness temperatures simulated with the M2013 model using these parameters. From a first visual inspection of the time series, the following may be observed:

1. At the beginning of the simulations, the T2011 simulations for horizontal polarization exhibit a very high variability and show very high values.

2. In general, the T2011 model simulations show a higher variability of brightness temperatures at both polarizations than the simulations with the M2013 model.

3. In the first part of simulation No. 3, the snow density takes very high values, up to >900 kg m^{-3}, causing the brightness temperature at horizontal polarization to decrease considerably, according to both the T2011 and the M2013 model. These high density values occur when a precipitation event coincides with air temperatures above 0°C. The resulting precipitation is assumed to be rain, which then freezes when the temperature falls below 0°C, so the considered layer has the density of pure ice. However, as there is no mechanism for drainage in the model, it treats this layer as snow.

In order to further investigate the brightness temperatures modeled with the T2011 and the M2013 model, and the main factors controlling their evolution, we take all brightness temperatures from all six simulations and all time steps to compare the results. However, due to findings 1 and 3 above, we exclude some simulations from the correlation analysis below: The T2011 simulations start with a prescribed initial profile and need some time to adjust to the observed situation. Thus, we exclude the brightness temperature simulations of the first 100 time steps, i.e. of the first 25 days. Additionally, because the simulations with very high snow densities behave exceptionally, we exclude simulations with $\rho_{snow} > 600$ kg m^{-3} from the correlation analysis.

A more quantitative analysis reveals the following findings and their implications for further comparisons:

1. At horizontal polarization, the T2011 brightness temperatures can be divided roughly into two regimes if we consider the ice covered by a relatively thin and light snow layer separately from the ice covered by a snow layer with a high density and/or thickness. The separation appears to be most successful (in terms of explaining the resulting two distinct clusters of brightness temperatures) when we divide the simulations into two approximately commensurate clusters by separating the simulations assigned a snow density of $\rho_{snow} \leq 400$ kg m^{-3} and a snow thickness of $d_{snow} \leq 0.25$ m from the remaining simulations (Fig. 3).

2. In the M2013 model, the snow/ice interface temperature $T_{SNOW-ICE}$ is almost a linear function of the surface temperature $T_{SURFACE}$ of the snow-covered sea ice, while in the T2011 model, $T_{SNOW-ICE}$ is influenced more by other parameters (Fig. 4). Separating the results for a
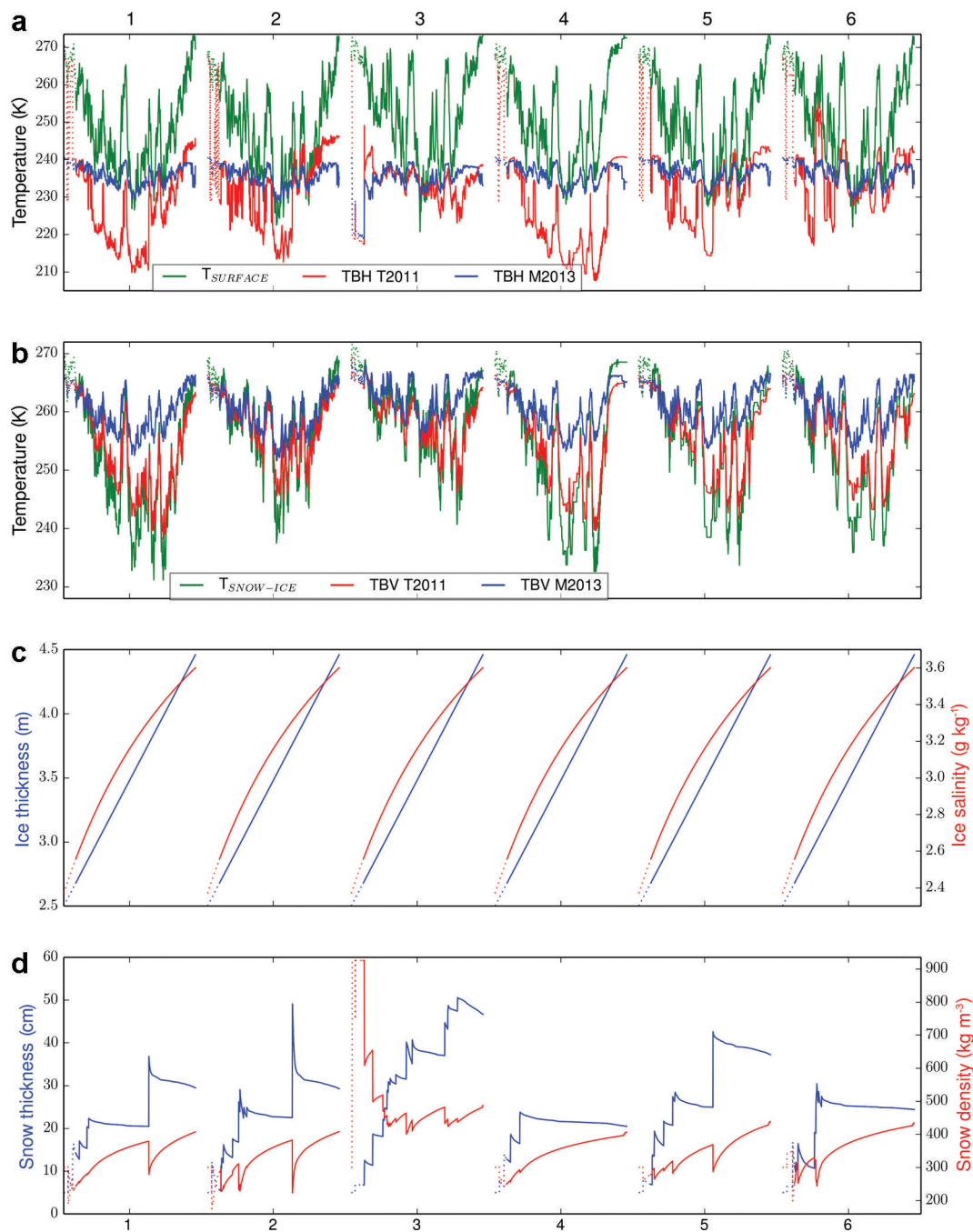
Fig. 2. Time series for the six T2011 model simulations every 6 hours from 1 September 1999 to 31 May 2000. Numbers 1–6 refer to the locations given in Figure 1. (a) The horizontally polarized brightness temperature (TBH) at 1.4 GHz ($\theta = 50°$), as obtained from the T2011 (red) and the M2013 model (blue; Tb), as well as the T2011 simulations of surface temperature T_{SURFACE} (green). (b) The brightness temperatures at vertical polarization (T2011 in red, M2013 in blue; Tb) and the snow/ice interface temperature $T_{\text{SNOW–ICE}}$ from the T2011 model (green). (c) The T2011 simulations of ice thickness (blue) and ice salinity (red). (d) The T2011 snow thickness (blue) and snow density (red). The parameters in (c, d) are used as input parameters to the M2013 model for all simulations, while T_{SURFACE} is used as input for the M2013 simulations denoted with Tb and both, T_{SURFACE} and $T_{\text{SNOW–ICE}}$, for the M2013 simulations denoted with Tb^*. The dotted lines indicate the results from the first 100 time steps of the simulations, of which the simulated brightness temperatures are excluded from the analysis (but shown in Figs 6 and 7).

relatively light and thin snow cover from the remaining cases leads to a distinct separation of $T_{\text{SNOW–ICE}}$ as a function of T_{SURFACE} in the M2013 model, but not in the T2011 model. As mentioned before, due to the different approaches used to determine $T_{\text{SNOW–ICE}}$ (and thus the ice temperature) in the two models, we either use both T_{SURFACE} and $T_{\text{SNOW–ICE}}$ from the T2011 simulations (Tb^*; see Figs 5–7), or only T_{SURFACE} from the T2011 simulations (Tb; see Table 1; Figs 2 and 8), as input to the M2013 model.

The comparison of all brightness temperatures at horizontal polarization as obtained from the T2011 and the M2013 emission model (Tb^*) confirms that the T2011 simulations cover a broader range of brightness temperature values (Fig. 5). Separating the simulations with respect to their snow density and snow thickness appears to explain the two observed clusters. The coefficients of determination, i.e. the squared correlation coefficients (Fig. 5), are $r^2 = 0.84$ for simulations with a relatively light and thin snow cover and 0.53 for the remaining simulations. At vertical polarization,
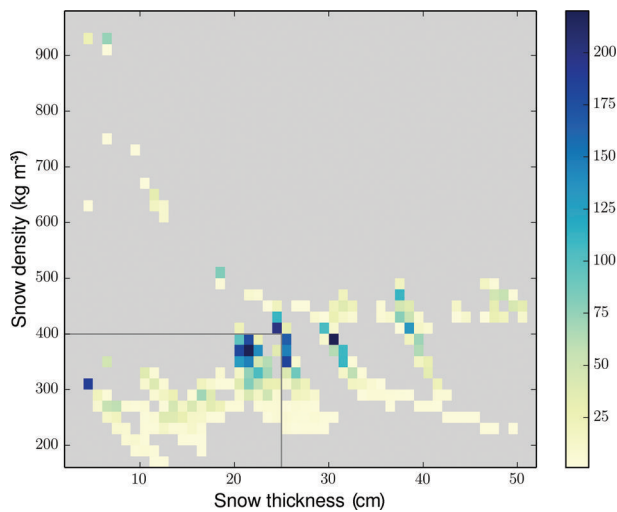
Fig. 3. Two-dimensional histogram of the snow density and snow thickness values as they occur for all six locations and times during the T2011 simulations. The box indicates the cases with a relatively light and thin snow cover ($\rho_{snow} \leq 400$ kg m^{-3} and $d_{snow} \leq 0.25$ m), which are considered separately in the following.

snow density and snow thickness have a negligible impact on brightness temperatures (Fig. 5), and we determine only one coefficient of determination. The vertically polarized brightness temperatures from the T2011 and the M2013 model agree better ($r^2 = 0.95$) than the horizontally polarized brightness temperatures. Yet, at vertical polarization, brightness temperatures in the M2013 model are generally higher than in the T2011 model, and their difference increases with decreasing brightness temperature. For comparison, if we use only the surface temperature from the T2011 model as input to the M2013 model and estimate ice temperature with the simple heat transfer equation given in the M2013 model, agreement between the brightness temperatures from the M2013 (Tb) and the T2011 model is lower, as indicated, for example, by the corresponding coefficients of determination, which are $r^2 = 0.72$ and 0.34 at horizontal polarization, and 0.65 at vertical polarization (compared to 0.84, 0.53 and 0.95 for Tb^*).

The next step is to identify which ice parameters mainly determine brightness temperature. At horizontal polarization, the brightness temperature in the M2013 model (Tb^*) is mainly determined by $T_{SNOW-ICE}$ (Fig. 6), and thus, because we assume a linear temperature gradient within the ice, by bulk ice temperature. If we assume a linear relationship between $T_{SNOW-ICE}$ and brightness temperature, $T_{SNOW-ICE}$ explains 95% of brightness temperature variability for the simulations considered here (i.e. $r^2 = 0.95$). For comparison, if we do not use $T_{SNOW-ICE}$ as an input to the M2013 model, but instead estimate $T_{SNOW-ICE}$ from $T_{SURFACE}$ and the ice conditions, using the simple heat equation in the M2013 model, the relationship between $T_{SNOW-ICE}$ and horizontally polarized M2013 brightness temperature (Tb) is weaker ($r^2 = 0.61$). For the T2011 model, the impact of $T_{SNOW-ICE}$ on the horizontally polarized brightness temperature is lower (Fig. 6) than for the M2013 model, although $T_{SNOW-ICE}$ can still be interpreted as accounting for more than half of the brightness temperature variability: $r^2 = 0.89$ for cases with a relatively light and thin snow cover and 0.55 for the remaining cases. Because, at vertical polarization, cases with a relatively light and thin snow cover do not differ from
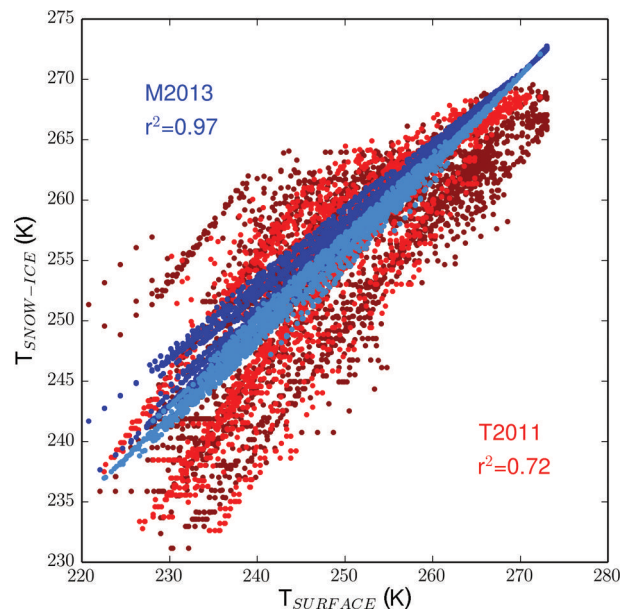

Fig. 4. Surface temperature $T_{SURFACE}$ versus snow/ice interface temperature $T_{SNOW-ICE}$ as obtained from the T2011 model (reddish colors) and as obtained from the M2013 model (bluish colors), respectively. Lighter colors indicate cases where the ice is covered by a relatively light and thin snow cover (see Fig. 3).

the remaining cases, we consider all simulations together in Figure 7. Both models suggest that brightness temperature at vertical polarization is almost solely a function of $T_{SNOW-ICE}$: the coefficients of determination for the two parameters are $r^2 = 0.97$ for the T2011 model and 0.99 for the M2013 model (Tb^*). For comparison, r^2 is 0.73 if only $T_{SURFACE}$ is used as input to the M2013 model (Tb). For high snow/ice interface temperatures, the brightness temperatures from the two models are similar, while the difference increases for lower snow/ice interface temperatures (Fig. 7).

Impact of ice parameters on potential snow thickness retrieval

Here we investigate the differences between the two models in terms of the potential for snow thickness retrieval from L-band brightness temperatures and the impact of ice conditions. In the M2013 model, the relationship between surface temperature and ice temperature is mainly determined by snow thickness, and this dependence was the basis for a first retrieval of snow thickness from L-band brightness temperatures over thick sea ice (Maaß and others, 2013). Thus, we now consider the M2013 brightness temperatures as simulated for the surface temperatures from the T2011 simulations and for the ice temperature as estimated within the M2013 model (Tb). In the first part of this section, we found that ice temperature is the main ice parameter influencing brightness temperature. In order to exclude the influence of the surface temperature, we keep it at a constant value by selecting only data with specific surface temperatures from the whole simulation dataset. Thus, we try to investigate which of the remaining ice parameters significantly influence brightness temperature.

Correlation analyses (not shown here) indicate that the main factors influencing the simulated brightness temperatures and the ice temperature are snow thickness d_{SNOW}, ice thickness d_{ICE} and snow density ρ_{SNOW}. In order to further investigate these parameters, we proceed as follows:
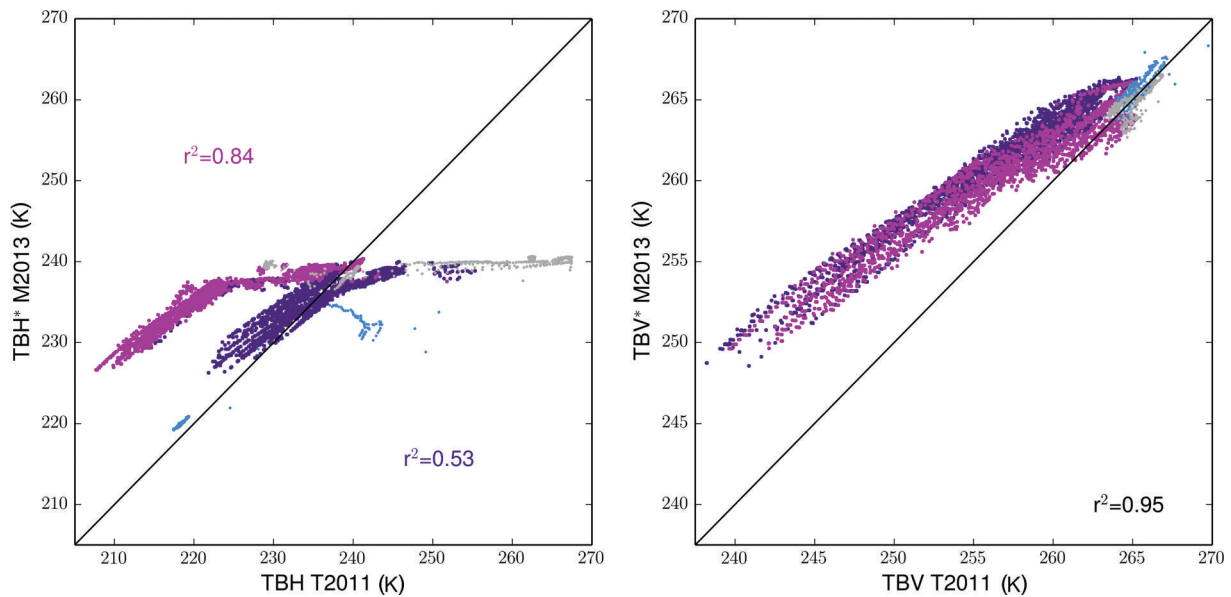
Fig. 5. Horizontally (left) and vertically (right) polarized brightness temperatures as obtained from the T2011 model and as obtained from the M2013 model (Tb^*), respectively. Light purple colors indicate cases where the ice is covered by a relatively light and thin snow layer, while dark purple colors indicate cases where the ice is covered by a heavier or thicker snow layer (see Fig. 3). Blue dots indicate cases with high snow densities $\rho_{snow} > 600 \, kg \, m^{-3}$, and gray dots indicate simulations from the first 100 time steps, which are shown as dotted lines in Figure 2. The simulations indicated by the blue or gray dots are excluded from the further analysis.

In the considered cases, the total ranges of values are $d_{SNOW} = 0.05...0.50 \, m$, $d_{ICE} = 2.7...4.5 \, m$, and $\rho_{SNOW} = 200...500 \, kg \, m^{-3}$. For each parameter ($d_{SNOW}$, d_{ICE} or ρ_{SNOW}), we select from the simulation dataset only the data associated with an almost constant surface temperature ($\pm 1 \, K$) and with roughly constant values for the two remaining parameters. This latter requirement is instantiated by selecting only the data in which these two remaining parameters are within 13–15% of their total variabilities (i.e. $\pm 0.033 \, m$ for d_{SNOW}, $\pm 0.135 \, m$ for d_{ICE} and $\pm 20 \, kg \, m^{-3}$ for ρ_{SNOW}). We then take into account all cases in which the considered parameter varies by at least 40% of its total variability and in which we find more than 50 simulations.

For these cases, we calculate the coefficients of determination between the T2011 simulations for the considered ice parameter (d_{SNOW}, d_{ICE} or ρ_{SNOW}) and the brightness temperatures from the T2011 and the M2013 model. Additionally, we calculate the coefficient of determination between the considered ice parameter and the snow/ice interface temperatures as obtained from the two models. We use the average coefficients of determination as rough estimations of the considered parameter's impact (Table 1). However, we find that the coefficients of determination are not very stable. If we change the maximum range for the parameters that are supposed to be constant, the minimum range for the considered parameter, or the minimum number
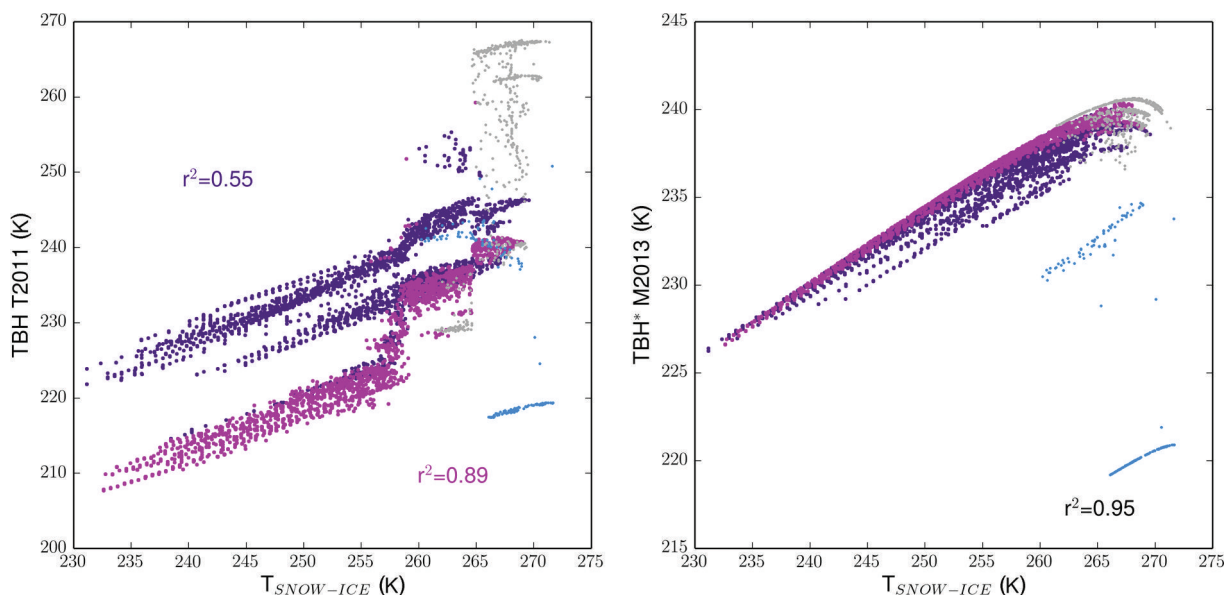

Fig. 6. Horizontally polarized brightness temperatures as obtained from the T2011 model (left) and as obtained from the M2013 model (Tb^*; right) versus the snow/ice interface temperature $T_{SNOW-ICE}$. Colors are explained in the Figure 5 caption.

of simulations found for each case, the values of the coefficients of determination change significantly. Thus, the presented values should be interpreted with caution. At horizontal polarization, the correlation analyses for the two models agree in that brightness temperature has the highest correlation with snow thickness and the lowest with snow density, when the respective remaining parameters are kept constant. In contrast, at vertical polarization, the M2013 model suggests a high correlation with snow thickness ($r^2 = 0.82$), while the correlation with snow thickness is low in the T2011 model ($r^2 = 0.09$), and the highest value for the T2011 model is found for ice thickness ($r^2 = 0.37$). As for brightness temperatures, the snow/ice interface temperature is mainly explained by snow thickness in the M2013 model ($r^2 = 0.83$), followed by ice thickness ($r^2 = 0.36$). In contrast, according to the T2011 model, correlations with all three considered parameters (d_{SNOW}, d_{ICE}, ρ_{SNOW}) are relatively low. The two models agree relatively well regarding the dependency between the horizontally polarized brightness temperature and the snow thickness, suggesting that it may be possible to extract information on the snow thickness of thick sea ice from SMOS measurements. Thus, in Figure 8 the relationship between brightness temperature at horizontal polarization and snow thickness is shown for four different ice conditions (in terms of surface temperature, snow density and ice thickness).

Compared to the results in Table 1, the constraints on surface temperature (± 2 K) and ice thickness (± 0.20 m) are somewhat less restrictive in Figure 8 (see figure caption), and each example contains between 126 and 192 single simulations. Additionally, the coefficients of determination for these examples are calculated with respect to a root function (see Fig. 8 caption). For all four considered ice conditions, brightness temperatures in the T2011 model increase more steeply with snow thickness than in the M2013 model. The coefficients of determination are between 0.43 and 0.84 with respect to a root function (see Fig. 8), and 0.02 lower each with respect to a linear function (not shown here).

DISCUSSION AND CONCLUSIONS

We found that over thick sea ice, brightness temperatures at horizontal and vertical polarization as modeled with the relatively simple M2013 model are mainly determined by ice temperature, which in turn is an almost linear function of surface temperature. If the surface temperature is constant, the ice temperature is mainly controlled by snow thickness, so brightness temperatures at both polarizations depend on
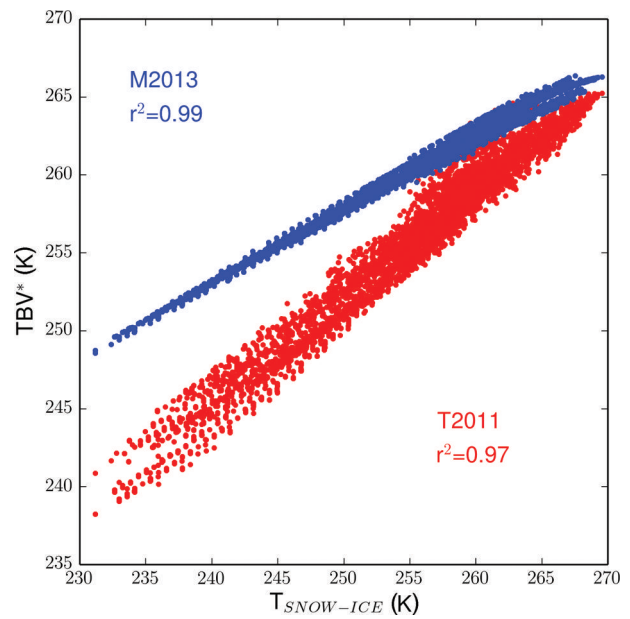

Fig. 7. Vertically polarized brightness temperatures as obtained from the T2011 model (red) and as obtained from the M2013 model (blue; Tb^*) versus the snow/ice interface temperature $T_{SNOW-ICE}$.

snow thickness. Thus, according to the M2013 model, snow thickness appears to be retrievable from L-band brightness temperatures at 50° incidence angle at both polarizations, if the surface temperature is known. In the more sophisticated T2011 model, vertically polarized brightness temperatures are mainly determined by ice temperature, as in the M2013 model, whereas brightness temperatures at horizontal polarization are also influenced by other ice parameters. Because the relationship between ice temperature and ice conditions is more complex in the T2011 than in the M2013 model, the correlation between brightness temperature at vertical polarization and snow thickness is relatively weak in the T2011 model. However, brightness temperatures at horizontal polarization appear to depend on snow thickness, suggesting that the retrieval of snow thickness from L-band brightness temperatures at horizontal polarization is possible if information on the surface temperature is available (here within the range ± 2 K), and some assumptions about ice thickness (here within the range ± 0.20 m) and snow density (here within the range ± 20 kg m^{-3}) can be made. In contrast to higher microwave frequencies (Willmes and others, 2013), we did not find significant correlations between 1.4 GHz brightness temperatures and the scatterer correlation length, which is related to snow grain size, or snow

Table 1. Average coefficients of determination r^2 between brightness temperatures obtained from the T2011 model (denoted by superscript T) and the M2013 model (denoted by superscript M) at horizontal (TBH) and vertical (TBV) polarization with respect to snow thickness d_{SNOW}, ice thickness d_{ICE} and snow density ρ_{SNOW}, respectively. For each parameter the two remaining parameters are kept almost constant. Additionally, the average r^2 between the snow/ice interface temperature $T_{SNOW-ICE}$ (denoted by T_{SI}) and d_{SNOW}, d_{ICE} and ρ_{SNOW} are given. N is the number of simulations found for the criteria. The r^2 values are significant at the 99% level, unless a different value is given in parentheses

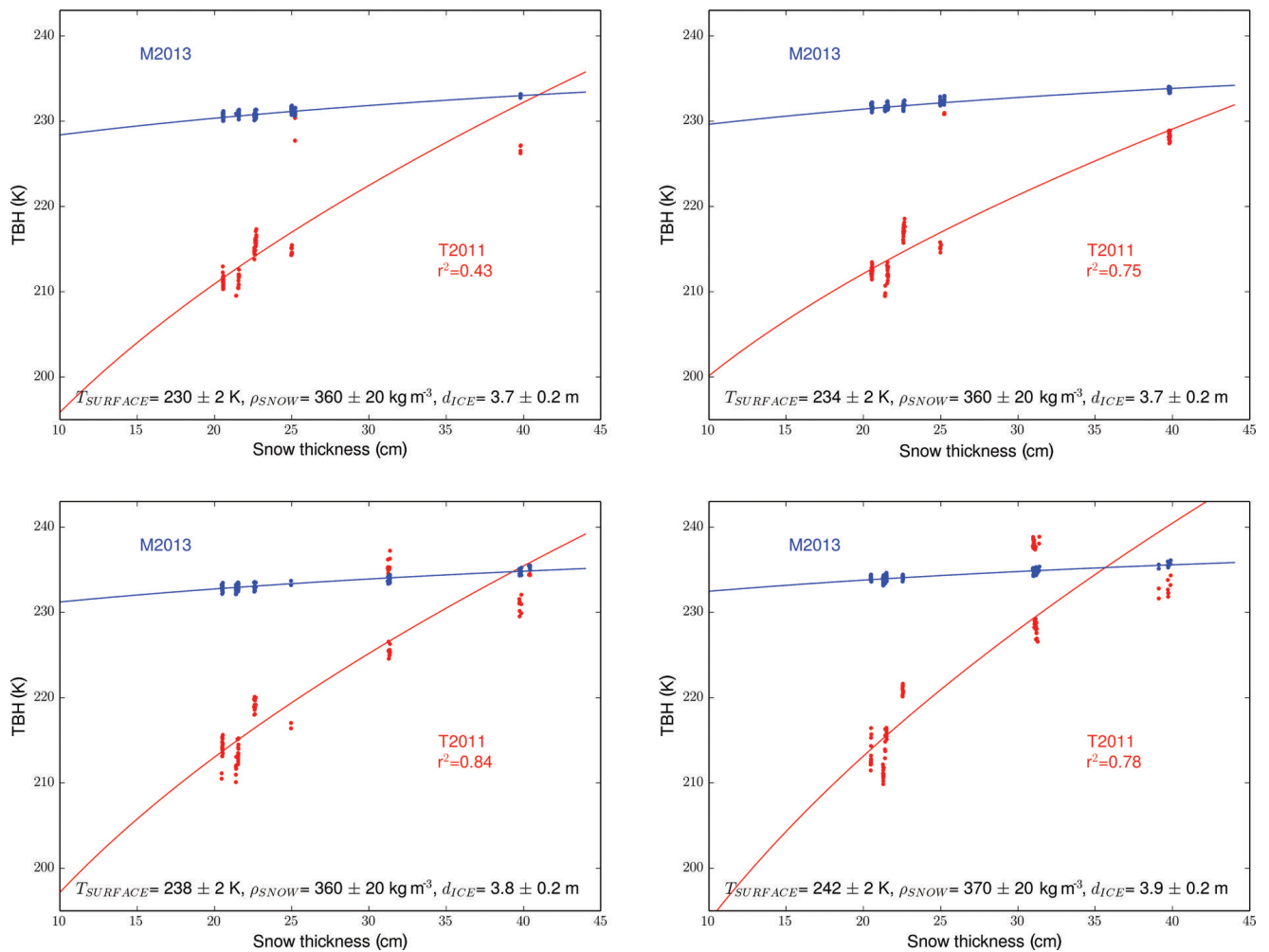|	TBH^T	TBH^M	TBV^T	TBV^M	T_{SI}^T	T_{SI}^M	N
d_{SNOW}	0.55	0.78	0.09 (92%)	0.82	0.05 (80%)	0.83	35
d_{ICE}	0.35	0.51	0.37	0.30	0.19 (98%)	0.36	28
ρ_{SNOW}	0.04 (54%)	0.20 (94%)	0.04 (54%)	0.52	0.04 (54%)	0.04 (54%)	16

Fig. 8. Horizontally polarized brightness temperatures as obtained from the T2011 model (red) and as obtained from the M2013 model (*Tb*; blue) versus the snow thickness for ice surface temperature (T_{SURFACE}), snow density (ρ_{SNOW}) and ice thickness (d_{ICE}) values selected as given in the figure. The blue line is the brightness temperature as a function of the snow thickness as modeled with the M2013 model for the average values of T_{SURFACE}, ρ_{SNOW} and d_{ICE}. The red line is a fitted curve for the T2011 results and has the form $Tb = a + b \cdot \sqrt{d_{\text{snow}}}$; the given coefficients of determination are calculated with respect to the corresponding fitted curves.

surface density, for example. Surface roughness may have an impact on L-band brightness temperatures; however, with the considered emission models in their current states we cannot investigate this. In addition to the snow thickness retrieval uncertainty due to the assumptions about ice conditions, SMOS measurements contain radiometric noise. The radiometric accuracy of single SMOS measurements is about 2.1–2.4 K (personal communication from M. Martin-Neira, 2013). While brightness temperature sensitivity to snow thickness as suggested by the M2013 model (about 3–4 K for a snow thickness increase of 0.30 m) thus implies the need for extensive temporal and spatial averaging of SMOS data, the radiometric accuracy appears to be a minor source of uncertainty according to the average sensitivity suggested by the T2011 model (about 30–40 K for a snow thickness increase of 0.30 m). However, the T2011 model showed higher variability for individual brightness temperature simulations than the M2013 model because the simulations are influenced by more parameters and consider multiple layers within the snow and ice.

Our results for the more sophisticated T2011 model (Tonboe and others, 2011) appear to confirm that brightness temperatures at horizontal polarization increase with snow thickness, even more clearly than in the previously used

retrieval model M2013 (Maaß and others, 2013). In contrast, vertically polarized brightness temperatures in the T2011 model were almost independent of snow thickness. Thus, although brightness temperatures at vertical polarization showed better agreement between the two models, we conclude that a potential SMOS snow thickness retrieval should be based on data at horizontal polarization. Our comparison of the two models suggests that the simpler M2013 model may benefit from a more sophisticated implementation of the relationship between surface temperature and ice temperature. Alternatively, the snow/ice interface temperature may be inferred from Advanced Microwave Scanning Radiometer (AMSR) measurements at 6 GHz (Tonboe and others, 2011) and could be an independent input parameter to the SMOS retrieval model. For monitoring long-term changes in the Arctic, a combined ice and snow thickness product would be desirable and could be accomplished as follows: For CryoSat-2 ice thickness measurements, the uncertainty decreases with ice thickness (e.g. Alexandrov and others, 2010), while it generally increases with ice thickness (and temperature) in the SMOS ice thickness retrieval. The CryoSat-2 and SMOS error estimations could thus be used to produce an error-weighted combined ice thickness map. Over thick ice, the

CryoSat-2 data could also be used as a rough estimation of ice thickness for the SMOS snow thickness retrieval, which could then possibly be used to (iteratively) refine the CryoSat-2 ice thickness retrieval. While AMSR measurements could provide some information on the snow/ice interface temperature, information on the (snow) surface temperature could be obtained from Moderate Resolution Imaging Spectroradiometer (MODIS) measurements (Hall and others, 2004). Including these supplementary satellite data may be beneficial for both the SMOS ice and snow thickness retrieval. Finally, AMSR-based snow thicknesses over (thinner) first-year ice could complement the SMOS-retrieved snow thicknesses over (thicker) multi-year ice.

ACKNOWLEDGEMENTS

REFERENCES

Alexandrov V, Sandven S, Wahlin J and Johannessen OM (2010) The relation between sea ice thickness and freeboard in the Arctic. *Cryosphere*, **4**(3), 373–380 (doi: 10.5194/tc-4-373-2010)

Burke WJ, Schmugge T and Paris JF (1979) Comparison of 2.8- and 21-cm microwave radiometer observations over soils with emission model calculations. *J. Geophys. Res.*, **84**(C1), 287–294 (doi: 10.1029/JC084iC01p00287)

Comiso JC, Cavalieri DJ and Markus T (2003) Sea ice concentration, ice temperature, and snow depth using AMSR-E data. *IEEE Trans. Geosci. Remote Sens.*, **41**(2), 243–252 (doi: 10.1109/TGRS.2002.808317)

Cox GFN and Weeks WF (1983) Equations for determining the gas and brine volumes in sea-ice samples. *J. Glaciol.*, **29**(102), 306–316

Giles KA and 8 others (2007) Combined airborne laser and radar altimeter measurements over the Fram Strait in May 2002. *Remote Sens. Environ.*, **111**(2–3), 182–194 (doi: 10.1016/j.rse.2007.02.037)

Hall DK, Key J, Casey KA, Riggs GA and Cavalieri DJ (2004) Sea ice surface temperature product from MODIS. *IEEE Trans. Geosci. Remote Sens.*, **42**(5), 1076–1087 (doi: 10.1109/TGRS.2004.825587)

Hezel PJ, Zhang X, Bitz CM, Kelly BP and Massonnet F (2012) Projected decline in spring snow depth on Arctic sea ice caused by progressively later autumn open ocean freeze-up this century. *Geophys. Res. Lett.*, **39**(17), L17505 (doi: 10.1029/2012GL052794)

Huntemann M, Heygster G, Kaleschke L, Krumpen T, Mäkynen M and Drusch M (2014) Empirical sea ice thickness retrieval during the freeze-up period from SMOS high incident angle observations. *Cryosphere*, **8**(2), 439–451 (doi: 10.5194/tc-8-439-2014)

Kaleschke L, Tian-Kunze X, Maaß N, Mäkynen M and Drusch M (2012) Sea ice thickness retrieval from SMOS brightness temperatures during the Arctic freeze-up period. *Geophys. Res. Lett.*, **39**(5), L05501 (doi: 10.1029/2012GL050916)

Klein L and Swift C (1977) An improved model for the dielectric constant of sea water at microwave frequencies. *IEEE Trans.*

Antennas Propag., **25**(1), 104–111 (doi: 10.1109/TAP.1977.1141539)

Kurtz NT and Farrell SL (2011) Large-scale surveys of snow depth on Arctic sea ice from Operation IceBridge. *Geophys. Res. Lett.*, **38**(20), L20505 (doi: 10.1029/2011GL049216)

Kwok R and Cunningham GF (2008) ICESat over Arctic sea ice: estimation of snow depth and ice thickness. *J. Geophys. Res.*, **113**(C8), C08010 (doi: 10.1029/2008JC004753)

Kwok R and 6 others (2011) Airborne surveys of snow depth over Arctic sea ice. *J. Geophys. Res.*, **116**(C11), C11018 (doi: 10.1029/2011JC007371)

Maaß N, Kaleschke L, Tian-Kunze X and Drusch M (2013) Snow thickness retrieval over thick Arctic sea ice using SMOS satellite data. *Cryosphere*, **7**(6), 1971–1989 (doi: 10.5194/tc-7-1971-2013)

Markus T and Cavalieri DJ (1998) Snow depth distribution over sea ice in the Southern Ocean from satellite passive microwave data. In Jeffries MO ed. *Antarctic sea ice: physical processes, interactions and variability.* (Antarctic Research Series 74) American Geophysical Union, Washington, DC, 19–39

Maykut GA and Untersteiner N (1971) Some results from a time-dependent thermodynamic model of sea ice. *J. Geophys. Res.*, **76**(6), 1550–1575 (doi: 10.1029/JC076i006p01550)

Mecklenburg S and 10 others (2012) ESA's soil moisture and ocean salinity mission: mission performance and operations. *IEEE Trans. Geosci. Remote Sens.*, **50**(5), 1354–1366 (doi: 10.1109/TGRS.2012.2187666)

Pounder ER (1965) *The physics of ice.* Pergamon Press, Oxford

Screen JA and Simmonds I (2012) Declining summer snowfall in the Arctic: causes, impacts and feedbacks. *Climate Dyn.*, **38**(11–12), 2243–2256 (doi: 10.1007/s00382-011-1105-2)

Stroeve JC and 8 others (2006) Impact of surface roughness on AMSR-E sea ice products. *IEEE Trans. Geosci. Remote Sens.*, **44**(11), 3103–3117 (doi: 10.1109/TGRS.2006.880619)

Tian-Kunze X and 6 others (2013) SMOS derived sea ice thickness: algorithm baseline, product specifications and initial verification. *Cryosphere*, **8**(3), 997–1018 (doi: 10.5194/tc-8-997-2014)

Tiuri MT, Sihvola AH, Nyfors EG and Hallikainen MT (1984) The complex dielectric constant of snow at microwave frequencies. *IEEE J. Ocean. Eng.*, **9**(5), 377–382 (doi: 10.1109/JOE.1984.1145645)

Tonboe RT, Heygster G, Pedersen LT and Andersen S (2006) Sea ice emission modelling. In Mätzler C ed. *Thermal microwave radiation: applications for remote sensing.* (IET Electromagnetic Waves Series 52) Institution of Engineering and Technology, London, 382–400

Tonboe RT, Dybkjær G and Høyer JL (2011) Simulations of the snow covered sea ice surface temperature and microwave effective temperature. *Tellus A*, **63**(5), 1028–1037 (doi: 10.1111/j.1600-0870.2011.00530.x)

Untersteiner N (1964) Calculations of temperature regime and heat budget of sea ice in the central Arctic. *J. Geophys. Res.*, **69**(22), 4755–4766 (doi: 10.1029/JZ069i022p04755)

Vant MR, Ramseier RO and Makios V (1978) The complex-dielectric constant of sea ice at frequencies in the range 0.1–40 GHz. *J. Appl. Phys.*, **49**(3), 1264–1280 (doi: 10.1063/1.325018)

Warren SG and 6 others (1999) Snow depth on Arctic sea ice. *J. Climate*, **12**(6), 1814–1829 (doi: 10.1175/1520-0442(1999)012<1814:SDOASI>2.0.CO;2)

Wiesmann A and Mätzler C (1999) Microwave emission model of layered snowpacks. *Remote Sens. Environ.*, **70**(3), 307–316 (doi: 10.1016/S0034-4257(99)00046-2)

Willmes S, Nicolaus M and Haas C (2013) The microwave emissivity variability of snow covered first-year sea ice from late winter to early summer: a model study. *Cryos. Discuss.*, **7**(6), 5711–5734 (doi: 10.5194/tcd-7-5711-2013)

Yu Y and Rothrock DA (1996) Thin ice thickness from satellite thermal imagery. *J. Geophys. Res.*, **101**(C11), 25 753–25 766 (doi: 10.1029/96JC02242)